Transcriptome analysis of distinct mouse strains reveals kinesin light chain-1 splicing as an amyloid-β accumulation modifier

Takashi Morihara[a,1,2], Noriyuki Hayashi[a,b,1], Mikiko Yokokoji[a,1], Hiroyasu Akatsu[c], Michael A. Silverman[a,d], Nobuyuki Kimura[e], Masahiro Sato[a], Yuhki Saito[f], Toshiharu Suzuki[f], Kanta Yanagida[a], Takashi S. Kodama[a], Toshihisa Tanaka[a], Masayasu Okochi[a], Shinji Tagami[a], Hiroaki Kazui[a], Takashi Kudo[a], Ryota Hashimoto[a,g], Naohiro Itoh[a], Kouhei Nishitomi[a], Yumi Yamaguchi-Kabata[h], Tatsuhiko Tsunoda[i], Hironori Takamura[j], Taiichi Katayama[j], Ryo Kimura[a,k], Kouzin Kamino[a,l], Yoshio Hashizume[c], and Masatoshi Takeda[a]

[a]Department of Psychiatry, Graduate School of Medicine, Osaka University, Osaka 565-0871, Japan; [b]Department of Complementary and Alternative Medicine, Graduate School of Medicine, Osaka University, Osaka 565-0871, Japan; [c]Choju Medical Institute, Fukushimura Hospital, Aichi 441-8124, Japan; [d]Department of Biological Sciences, Simon Fraser University, Burnaby, BC, Canada, V5A 1S6; [e]Section of Cell Biology and Pathology, Department of Alzheimer's Disease Research, Center for Development of Advanced Medicine for Dementia, National Center for Geriatrics and Gerontology, Aichi 474-8511, Japan; [f]Laboratory of Neuroscience, Graduate School of Pharmaceutical Sciences, Hokkaido University, Sapporo 060-0812, Japan; [g]Molecular Research Center for Children's Mental Development, United Graduate School of Child Development, Osaka University, Kanazawa University, Hamamatsu University School of Medicine, Chiba University and Fukui University, Osaka 565-0871, Japan; [h]Department of Integrative Genomics, Tohoku Medical Megabank Organization, Tohoku University, Miyagi 980-8575, Japan; [i]Laboratory for Medical Science Mathematics, RIKEN Center for Integrative Medical Sciences, Kanagawa 230-0045, Japan; [j]Department of Child Development & Molecular Brain Science, United Graduate School of Child Development, Osaka University, Osaka 565-0871, Japan; [k]Department of Anatomy and Developmental Biology, Graduate School of Medicine, Kyoto University, Kyoto 606-8501, Japan; and [l]National Hospital Organization, Yamato Mental Medical Center, Nara 639-1042, Japan

Edited by Robert W. Mahley, The J. David Gladstone Institutes, San Francisco, CA, and approved December 13, 2013 (received for review May 1, 2013)

Alzheimer's disease (AD) is characterized by the accumulation of amyloid-β (Aβ). The genes that govern this process, however, have remained elusive. To this end, we combined distinct mouse strains with transcriptomics to directly identify disease-relevant genes. We show that AD model mice (*APP*-Tg) with DBA/2 genetic backgrounds have significantly lower levels of Aβ accumulation compared with SJL and C57BL/6 mice. We then applied brain transcriptomics to reveal the genes in DBA/2 that suppress Aβ accumulation. To avoid detecting secondarily affected genes by Aβ, we used non-Tg mice in the absence of Aβ pathology and selected candidate genes differently expressed in DBA/2 mice. Additional transcriptome analysis of *APP*-Tg mice with mixed genetic backgrounds revealed kinesin light chain-1 *(Klc1)* as an Aβ modifier, indicating a role for intracellular trafficking in Aβ accumulation. Aβ levels correlated with the expression levels of *Klc1* splice variant E and the genotype of *Klc1* in these *APP*-Tg mice. In humans, the expression levels of *KLC1* variant E in brain and lymphocyte were significantly higher in AD patients compared with unaffected individuals. Finally, functional analysis using neuroblastoma cells showed that overexpression or knockdown of *KLC1* variant E increases or decreases the production of Aβ, respectively. The identification of *KLC1* variant E suggests that the dysfunction of intracellular trafficking is a causative factor of Aβ pathology. This unique combination of distinct mouse strains and model mice with transcriptomics is expected to be useful for the study of genetic mechanisms of other complex diseases.

mouse-to-human translation | alternative splicing

Alzheimer's disease (AD) is a common cause of dementia that is characterized by the accumulation of amyloid-β (Aβ) peptide. Its causes (especially of sporadic AD, which comprises the majority of AD cases), however, are still largely unknown, and no efficient treatment exists. Since the first AD risk gene, apolioprotein E *(APOE)*, was identified, over 1,300 genetic studies have been done (www.alzgene.org) (1), and ∼10,000 human genomic samples have identified AD risk genes (2–8). Regardless, these genes cannot account for the estimated 60–80% hereditary risk of AD (9). Also, they do not reveal their role in the cause of AD (10), because complex diseases, including AD, are often explained by the heterogeneity of diseases, uncontrollable environmental factors, and the complexity of human genome variation, which complicate conclusions from genome studies (11–13).

These limitations can be resolved by using mice. Mice with a mixed genetic background prepared from inbred mouse strains have simple genetic backgrounds, which drastically increase the statistical power for the identification of disease-related genes (14). AD is a complex disease not only genetically but also, neuropathologically and symptomatically (11), with its clinical diagnosis often ambiguous. Although increased Aβ levels in the brain are central to the pathology of AD, Aβ levels are difficult to measure in humans. In contrast, Aβ levels can be directly measured in mice. Furthermore, in human studies, although aging is the strongest risk

Significance

Genetic studies of common complex human diseases, including Alzheimer's disease (AD), are extremely resource-intensive and have struggled to identify genes that are causal in disease. Combined with the costs of studies and the inability to identify the missing heritability, particularly in AD, alternate strategies warrant consideration. We devised a unique strategy that combines distinct mouse strains that vary naturally in amyloid-β production with transcriptomics to identify kinesin light chain-1 *(Klc1)* splice variant E as a modifier of amyloid-β accumulation, a causative factor of AD. In AD patients, the expression levels of *KLC1* variant E in brain were significantly higher compared with levels in unaffected individuals. The identification of *KLC1* variant E suggests that dysfunction of intracellular trafficking is causative in AD.

Author contributions: T.M. and M.T. designed research; T.M., N.H., M.Y., H.A., N.K., M.S., K.Y., T.S.K., T. Tanaka, S.T., H.K., T. Kudo, R.H., H.T., T. Katayama, and Y.H. performed research; T.M., N.H., M.Y., N.K., M.S., Y.S., T.S., K.Y., T.S.K., T. Tanaka, N.I., K.N., H.T., T. Katayama, R.K., and K.K. contributed new reagents/analytic tools; T.M., N.H., M.Y., H.A., N.K., M.S., Y.Y.-K., and T. Tsunoda analyzed data; and T.M., M.A.S., and M.O. wrote the paper.

The authors declare no conflict of interest.

This article is a PNAS Direct Submission.

Freely available online through the PNAS open access option.

Data deposition: The transcriptome datasets reported in this paper have been deposited in the Gene Expression Omnibus (GEO) database, www.ncbi.nlm.nih.gov/geo (accession no. GSE40330).

[1]T.M., N.H., and M.Y. contributed equally to this work.

[2]To whom correspondence should be addressed. E-mail: morihara@psy.med.osaka-u.ac.jp.

This article contains supporting information online at www.pnas.org/lookup/suppl/doi:10.1073/pnas.1307345111/-/DCSupplemental.

factor for AD, it is not practical to collect same age samples or control for environmental factors. Mice, however, can be aged in equally controlled environments and analyzed at exactly the same age. Despite these significant advantages, most of the rodent genomic studies addressing human diseases, including AD, have not identified targets at the molecular level (15, 16). Thus, we applied transcriptomics: a straightforward approach to identify genes compared with conventional genome studies based on linkage disequilibrium between markers (17).

We first generated mice with different genetic backgrounds that accumulated varying amounts of Aβ. Then, instead of using standard genetic approaches, we performed genome-wide transcriptome analysis on the mice. We identified a specific splice form of kinesin light chain-1 (*Klc1*), variant E, as a modifier of the Aβ accumulation. Notably, the transcript levels of *KLC1* variant E were significantly higher in pathologically diagnosed AD patients with confirmed levels of excessive Aβ compared with controls. A functional role for KLC1 variant E was shown by manipulating its expression levels in neuroblastoma cells and showing that this variant can modulate Aβ production. This study shows that the central pathology of AD is modified by the splicing of *KLC1* and suggests that the combination of animal models and transcriptomics is an efficient approach to identifying key genes in common complex diseases.

Results

DBA/2 Genetic Backgrounds Suppress Aβ Levels in AD Model Mice. To examine the impact on Aβ accumulation by genetic background, we prepared amyloid precursor protein (*APP*)-Tg mice with mixed genetic backgrounds by crossing the Tg2576 mice with the phenotypically distinct strains C57BL/6 (B6), SJL, and DBA/2 (DBA). We obtained six groups of *APP*-Tg mice, and each group contained different mixture ratios of the three strains in their genetic background (Fig. 1*A*). We analyzed these *APP*-Tg mice at 12 mo of age to assess the effects on Aβ accumulation by genetic background (n = 59). The levels of Aβ40 and Aβ42 in a 1% Triton-X (Fig. 1 *B–D*) and 6 M guanidine HCl (GuHCl) (Fig. 1 *E–G*) fraction from brain were measured by ELISA. The levels of Aβ ranged more than 10-fold, and the mice carrying DBA alleles (dark blue and light blue) had lower amounts of Aβ

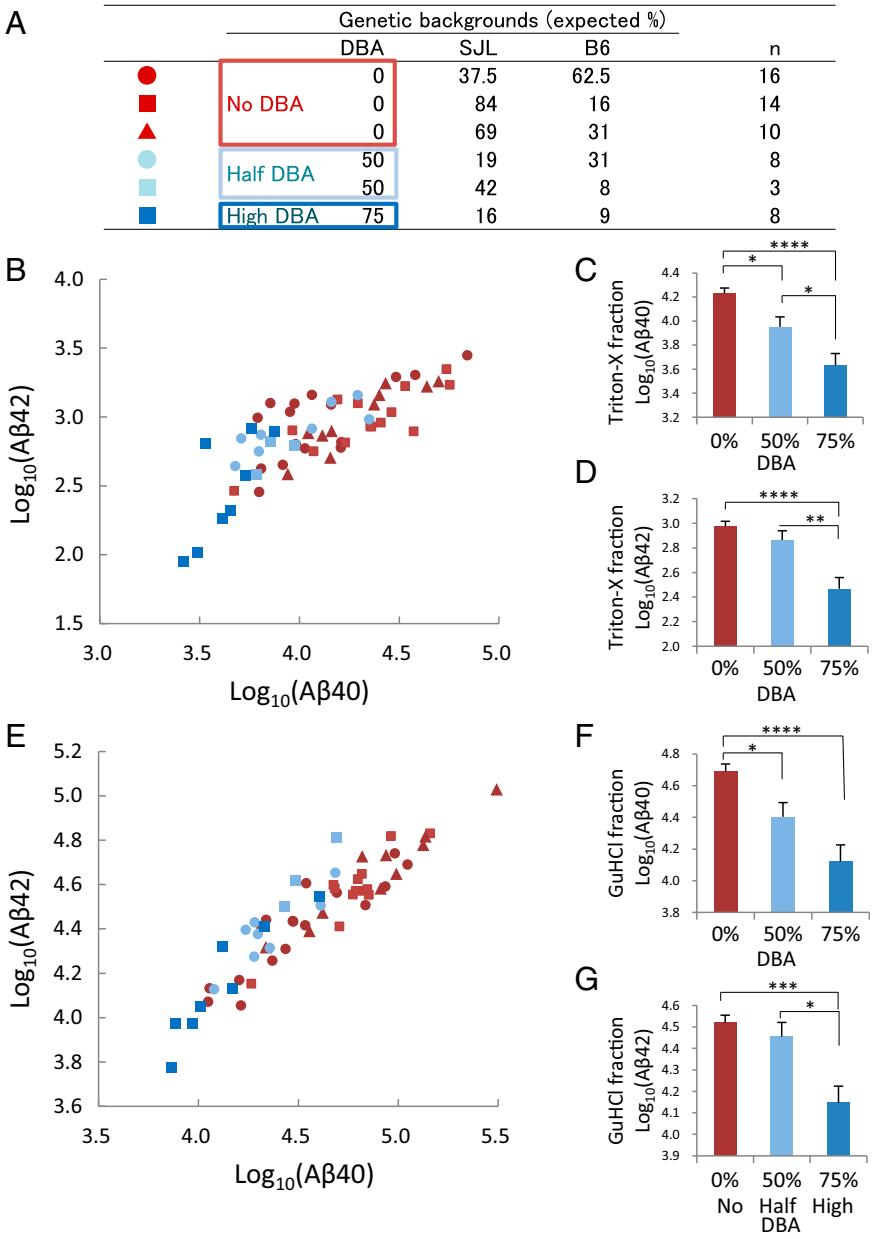

Fig. 1. Effects of the genetic background on Aβ accumulation in *APP*-Tg mouse brain. (*A*) The composition of *APP*-Tg mice with mixed genetic backgrounds. The colors indicate the expected percentage of DBA genetic background: 0% (red), mice carrying no DBA alleles (n = 40); 50% (light blue), mice carrying 50% DBA alleles (n = 11); and 75% (dark blue), mice carrying 75% DBA alleles (n = 8). Aβ levels in (*B–D*) 1% Triton-X and (*E–G*) 6 M GuHCl fractions as measured by ELISA. (*B* and *E*) Symbols denote Aβ40 and Aβ42 levels for individual *APP*-Tg mice with mixed genetic backgrounds. (*C*, *D*, *F*, and *G*) Aβ levels in mice with different percentages of DBA genetic background. (*C*) The mice carrying 75% DBA alleles (high DBA, dark blue) and 50% DBA alleles (one-half DBA, light blue) had lower Aβ [−74.7% (P < 0.0001) and −47.3% (P = 0.012), respectively] than mice carrying no DBA alleles (no DBA, red). (*D*) Likewise, the levels of Aβ42 in high DBA mice had lower Aβ accumulation compared with one-half DBA or no DBA mice [−59.5% (P = 0.0048) and −68.9% (P < 0.0001), respectively]. (*F*) Compared with Aβ40 levels in no DBA mice, Aβ40 levels in one-half DBA and high DBA mice were −48.4% (P = 0.017) and −73.1% (P < 0.0001) lower, respectively. (*G*) The levels of GuHCl Aβ42 in high DBA mice were −57.7% (P = 0.0002) and −50.8% (P = 0.011) lower compared with Aβ42 levels in no DBA and one-half DBA mice, respectively. *P < 0.05; **P < 0.01; ***P < 0.001; ****P < 0.0001 [Tukey–Kramer Honestly Significant Difference (HSD)]. Error bars indicate SEM. Aβ levels are shown in log10 scale (picograms Aβ per milligram total protein).

(Fig. 1 *B* and *E*). Compared with mice with no DBA alleles, the mice carrying 75% DBA alleles had lower levels of both forms of Aβ in these fractions (−74.7 to −57.7%, $P \leq 0.0001$–0.0002) (Fig. 1 *C*, *D*, *F*, and *G*). Notably, the expression levels of APP were not affected by the genetic backgrounds (Fig. S1). These findings drove us to search for the gene(s) in DBA mice that suppresses Aβ accumulation.

Mouse Transcriptomics Identify *Klc1* as a Modifier of Aβ Accumulation. Most previous mouse genomics studies (14, 15), including ones performed on AD (18, 19), failed to identify modifiers at the molecular level. Thus, instead of genomics, we applied transcriptomics, which is a more straightforward approach for identifying candidate molecules (17). We used 12 arrays for inbred mice (non-Tg) analyses and 28 arrays for the *APP*-Tg mice of mixed genetic backgrounds (Fig. 2*A*). First, 13,309 probes with signals that were reliably detectable in all 40 arrays (one mouse per array) were selected from 25,967 probes on the Illumina mouse Ref-8 Expression BeadChip. Second, to select the probes with expression levels that were affected by the DBA genetic background, we compared the expression levels of 13,309 probes in DBA, B6, and SJL inbred (non-Tg) mice (unpaired *t* test). Using inbred mice means that any change in gene expression is based on the genetic background and not secondary effects caused by Aβ accumulation. We applied strict criteria in this selection: the fold change had to be equal to or more than 1.5, and the false discovery rate was set to 0.001. In total, 54 probes were identified, with the signals of 47 probes being lower and the signals of 7 probes being higher in DBA mice than the signals in either B6 or SJL (Table S1).

In the final step, we examined the correlation between the expression levels of these 54 probes and Aβ40 levels in the GuHCl fraction in *APP*-Tg mice. Using strict selection criteria (Pearson product moment correlation false discovery rate = 0.001), we identified a total of four probes that correlated with Aβ levels. Notably, the two probes (probe IDs 4050133 and 6130468) that positively correlated with Aβ accumulation both detected the same transcript: *Klc1* (also known as *Kns2*) (Fig. 2*B*).

In addition to these two *Klc1* probes, the arrays have another three *Klc1* probes (Fig. S2) (probe IDs 540139, 4060520, and 7330358) that, although they did not pass our strict genome-wide screen, provide data still worth considering. Two probes (540139 and 4060520) showed lower signal levels in DBA compared with other inbred strains ($P < 0.0001$ before multiple testing correction) and correlated with levels of Aβ accumulation in *APP*-Tg mice ($P < 0.0001$ before multiple testing correction). Similar to the probes identified above, these probes detect exons with complex splicing patterns. By contrast, probe 7330358 was not affected by the mouse strain ($P = 0.91$ between DBA and B6, $P = 0.30$ between DBA and SJL) and did not correlate with Aβ levels ($P = 0.49$). This probe exists in a region common to all splice variants of *Klc1*. Thus, all four probes with signals that were suppressed by the DBA genetic background and correlated with Aβ levels are located in the splice region of *Klc1*. These findings indicate that a splice variant of *Klc1* might be involved in the mechanism of Aβ accumulation.

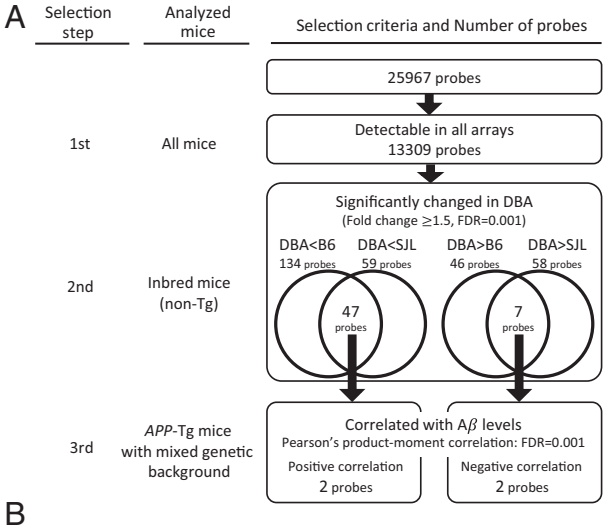

B

Gene name	Gene symbol	Illumina probe ID	Expression levels in DBA	Correlation with Aβ
kinesin light chain 1	***Klc1***	4050133	Low	Positive
kinesin light chain 1	***Klc1***	6130468	Low	Positive
gamma-aminobutyric acid (GABA-A) receptor, subunit beta 3	*Gabrb3*	14402	High	Negative
family with sequence similarity 20, member B	*Fam20b*	215015	High	Negative

Fig. 2. Genome-wide transcriptomics to identify Aβ modifiers in mice. (*A*) Candidate probes were narrowed down by three steps. In the first step, 13,309 probe with signals that were reliably detectable in all arrays were selected. In the second step, 47 probes with expression levels that were significantly lower in DBA inbred mice and seven probes with expression levels that were significantly higher in DBA compared with the other strains were selected for additional analysis [fold change ≥ 1.5; false discovery rate (FDR) = 0.001] (Table S1). In the third step, two probes with expression levels that were significantly and positively correlated with Aβ levels and two probes with expression levels that were significantly and negatively correlated with Aβ were ultimately identified (FDR = 0.001). (*B*) Probes identified by genome-wide transcriptomics for Aβ modifier genes. All array data are deposited in the Gene Expression Omnibus (accession no. GSE40330).

Levels of a Specific Splice Variant but Not Total *Klc1* Are Different in the DBA Strain. Because the array probes cannot distinguish the multitude of splice variants of *Klc1*, we developed variant-specific real-time quantitative PCR (QPCR) assays to identify which splice variant of *Klc1* modulates Aβ accumulation. We measured the mRNA expression levels of *Klc1* variants A–E in mouse hippocampus in addition to the total levels of *Klc1* expression by detecting the common region (exons 3 and 4) of all splice variants (*Klc1* All). To examine whether the expression levels of each *Klc1* variant were affected by the DBA genetic background independent of Aβ accumulation, we measured expression levels in inbred mice (non-Tg mice) at 6 ($n = 11$) and 12 mo of age ($n = 20$) (Fig. 3*A*). Consistent with the array results (probe ID 733035), there was no observed difference in the *Klc1* All expression levels among the three strains (DBA, SJL, and B6) at 6 (ANOVA: $P = 0.95$) or 12 mo of age (ANOVA: $P = 0.51$) (Fig. 3*A*, *Left*). In contrast to *Klc1* All, the expression levels of *Klc1* variant E were significantly lower in DBA mice than expression levels in SJL and B6 mice at both ages (Fig. 3*A*, *Right*). However, the *Klc1* splice variants A–D did not show consistent differences between DBA and the other two strains (Fig. S3).

***Klc1* Variant E but Not Total *Klc1* Correlates with the Levels of Aβ Accumulation.** To examine whether *Klc1* variant E affects Aβ accumulation in vivo, we measured the expression levels of *Klc1* variant E in *APP*-Tg mice with mixed genetic backgrounds ($n = 59$). The levels of *Klc1* variant E were significantly correlated with the levels of all forms of Aβ [Aβ40 (Pearson product moment correlation $R^2 = 0.39$, $P < 0.0001$; significant threshold with Bonferroni correction = 0.002) and Aβ42 ($R^2 = 0.24$, $P < 0.0001$) in the Triton fraction; Aβ40 ($R^2 = 0.33$, $P < 0.0001$) and Aβ42 ($R^2 = 0.21$, $P = 0.0002$) in the GuHCl fraction] (Fig. 3*B*, *Right*). In contrast, the expression levels of *Klc1* All and the other variants did not correlate with the levels of Aβ (except variant A but only with Aβ40 in Triton-X fractions) (Fig. 3*B*, *Left* and Fig. S4). The correlation between *Klc1* variant E and Aβ was unlikely caused by Aβ accumulation for many reasons, including no elevation of the levels of *Klc1* variant E in *APP*-Tg mice that had abundant Aβ compared with those Aβ in non-Tg littermates that had no Aβ pathology (Fig. S5). In addition to the array data (Fig. S2), these QPCR data (Fig. 3 *A* and *B* and Figs. S3, S4, and S5) suggested that splicing of *Klc1* was involved in the mechanisms of Aβ suppression by the DBA genetic background.

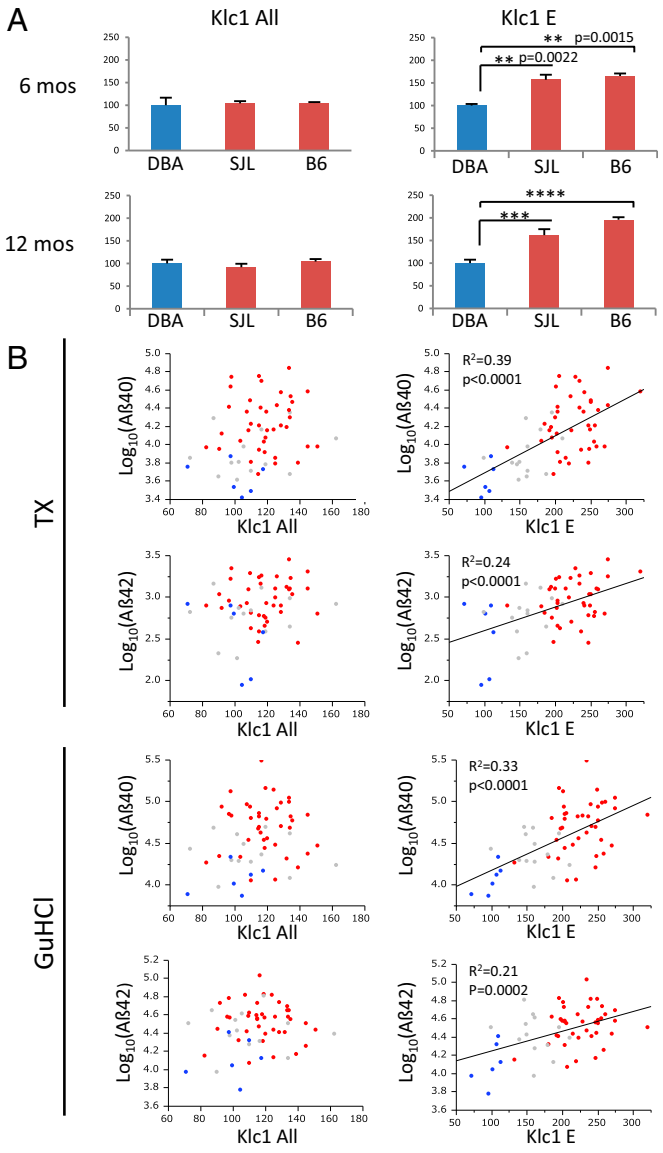

Fig. 3. *Klc1* splice variant E and the levels of Aβ. (*A*) Expression levels of *Klc1* variant E and *Klc1* All in three mouse strains (non-Tg mice). mRNA expression levels of (*Left*) *Klc1* All and (*Right*) *Klc1* E in each mouse strain at (*Upper*) 6 (n = 4 DBA, 4 SJL, and 3 B6) and (*Lower*) 12 mo of age (n = 7 DBA, 6 SJL, and 7 B6) were measured by QPCR. The expression levels in DBA were normalized to 100. Error bars indicate SEM. P values were calculated by the Tukey–Kramer HSD test and considered significant when they were less than 0.004 (0.05/12 tests) according to Bonferroni correction for multiple testing. $^{**}P < 0.01$; $^{***}P < 0.001$; $^{****}P < 0.0001$. (*B*) Relationship between the levels of Aβ accumulation and *Klc1* expression and number of DBA alleles of *Klc1* in *APP*-Tg mice with mixed genetic backgrounds. Expression levels of (*Left*) *Klc1* All and (*Right*) *Klc1* E in *APP*-Tg mice with mixed genetic backgrounds (n = 59) are shown on the x axis. Aβ40 and Aβ42 levels in Triton-X fraction (TX) and Aβ40 and Aβ42 levels in the GuHCl fraction in mouse brain are shown in log10 scale on the y axis (picograms Aβ per milligram total protein). Lines show the correlation between the levels of *Klc1* and Aβ. P values are considered significant when they are less than 0.002 (0.05/24 tests) according to Bonferroni correction for multiple testing. The color of dots indicates the genotype of *Klc1*: blue, mice carrying two *Klc1* alleles from DBA strain; gray, one *Klc1* allele from DBA; and red, no *Klc1* allele from DBA. The mean expression levels in mice carrying two DBA alleles were normalized to 100.

***Klc1* Allele in DBA Mice Decreases the Levels of *Klc1* Variant E and Aβ Accumulation in *APP*-Tg Mice with Mixed Genetic Backgrounds.** Because the genetic component of mRNA expression variation is often caused by differences produced by *cis*-acting polymorphisms (20), we genotyped the *Klc1* region of *APP*-Tg mice with mixed genetic backgrounds (Fig. 3*B*). As shown in the scatterplot of *Klc1* variant E (Fig. 3*B*, *Right*), mice with the same genotype clustered together. Mice carrying two DBA alleles in the *Klc1* region (Fig. 3*B*, blue) had the lowest levels of *Klc1* variant E expression and Aβ accumulation; mice carrying one DBA allele (Fig. 3*B*, gray) had intermediate levels, and mice carrying no DBA allele (Fig. 3*B*, red) had the highest levels of *Klc1* variant E expression and Aβ accumulation. These genotype data suggest that the expression of *Klc1* variant E was negatively dependent on the number of DBA alleles in the *Klc1* region and that this DBA allele of *Klc1* suppressed Aβ accumulation.

Although failing to identify any AD-related genes, two groups reported differences in Aβ levels among mouse strains (18, 19, 21). Collectively, these data suggest that B6 and SJL are high Aβ mouse strains and that A/J and DBA are low Aβ mouse strains (Fig. S6*A*, *Left*). We obtained SNP data from the mouse phenome database (www.jax.org/phenome) (22) to examine whether genomic variance in *Klc1* affects Aβ accumulation in these mouse strains. Remarkably, all SNP variation in *Klc1* distinguishes the two types of strains (high and low) (Fig. S6*A*), despite the fact that strains of a type are not the closest relatives to each other (Fig. S6*B*) (23).

KLC1 Variant E Affects Aβ Production in Neuroblastoma Cells. To test the direct effect on amyloid pathology by KLC1 variant E, we manipulated the expression levels of KLC1 variant E in neuroblastoma cells, collected the culture media, and assessed Aβ40 and Aβ42 production by ELISA. The overexpression of *Klc1* variant E into N2a cells increased both Aβ40 (+18.4 ± 3.4%, P = 0.0009) and Aβ42 (+9.27 ± 2.7%, P = 0.024) secretion (Fig. 4*A*). Next, we knocked down total levels of *KLC1* (KLC1 All siRNA), which includes *KLC1* variant E or *KLC1* variant E alone (KLC1 E siRNA) in SH-SY5Y cells (Fig. 4 *B* and *C*). The suppression of *KLC1* or *KLC1* variant E alone reduced both Aβ40 (−44.7 ± 2.6%, $P < 0.0001$ by KLC1 E siRNA) and Aβ42 secretion (−39.3 ± 0.6%, $P < 0.0001$ by KLC1 E siRNA) (Fig. 4*C*). These findings strengthen the causative role of KLC1 variant E in AD and suggest that aberrant splicing of *KLC1* impacts the accumulation of Aβ at the stage of its production.

Expression Levels of *KLC1* Variant E Are Higher in AD. Human and mouse *KLC1* splice variants share extensive similarities in not only amino acid sequence but also, exon composition (24) (Fig. S7), implying that each splice variant has an important function and is likely conserved between mouse and human. Thus, we measured the expression levels of *KLC1* variant E and *KLC1* All in the hippocampus of autopsy-confirmed AD (n = 10) and control patients (n = 14) (Table S2). Although those of *KLC1* All were not different between the two groups (P = 0.18) (Fig. 5*A*), the expression levels of *KLC1* variant E were significantly higher in AD (+30.7%, P = 0.0096 Student t test) compared with control subjects (Fig. 5*B*).

Gene expression profiles in peripheral blood and brain are reported to share similarities (20), thus we measured the levels of *KLC1* All and variant E by QPCR in peripheral lymphocyte from control (n = 17) and AD (n = 47) subjects (Table S3). Although the levels of *KLC1* All were not significantly different between the two (P = 0.56) (Fig. 5*C*), the expression levels of *KLC1* variant E were significantly higher in AD (+25.0%, P = 0.0013, Student t test) compared with control subjects (Fig. 5*D*). Because Aβ is not believed to accumulate in lymphocytes, the elevation of *KLC1* variant E expression levels was unlikely to be the result of Aβ deposition. Taken together, these data show that the levels of *KLC1* splice variant E but not total *KLC1* impact AD pathology in both humans and *APP*-Tg mice.

Discussion

By combining distinct mouse strains and model mice with transcriptome analysis, we identified a causative molecule in AD (*Klc1* splice variant E), finding that it accumulates with different levels of Aβ that are based on the different mouse genetic backgrounds.

GENETICS

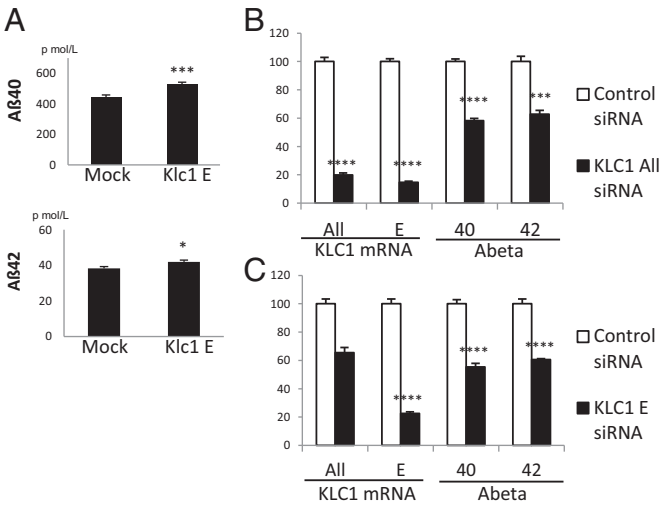

Fig. 4. The effects of *KLC1* variant E on Aβ production in neuroblastoma cells. (*A*) The levels of Aβ40 and Aβ42 in the culture medium after 72 h of Neuro2a transfected by mock control or *Klc1* variant E ($n = 11$ per group). (*B* and *C*) The relative levels of total mRNA levels of *KLC1* and *KLC1* variant E and the protein levels of Aβ40 and Aβ42 in the culture medium after 72 h of SH-SY5Y knocked down by (*B*) KLC1 All siRNA or KLC1 All control siRNA or (*C*) KLC1 E siRNA or KLC1 E control siRNA ($n = 4$ per group). $^{*}P < 0.05$; $^{**}P < 0.01$; $^{***}P < 0.001$; $^{****}P < 0.0001$ (Student *t* test without multiple testing correction). Error bars indicate SEM.

This finding is supported by multiple approaches, including mouse transcriptomics, mouse genome, human brain transcript, and human lymphocyte transcript analyses, along with functional analysis of KLC1 variant E in neuroblastoma cells.

Model mice with simple genetic backgrounds offer important advantages, such as controlled environmental factors and high detection power, which are amplified combined with transcriptional analysis. Complex diseases, including AD, show a continuum of clinical phenotypes, such as the levels of Aβ accumulation. Transcriptome analysis, therefore, is preferred, because it is highly concordant with the disease state and expected to provide an accurate molecular view of a complex disease (25). Additionally, although quantitative trait loci analysis and a genome-wide association study identify genetic markers, they do not point to specific genes, whereas transcriptomics does (17). In fact, thus far, less than 1% of rodent quantitative trait loci studies have identified molecular targets (14, 15). Finally, although the function of most genetic variation is unknown (10), gene expression variation offers clear functional targets.

The combination of transcriptional analysis and mice also minimizes the drawbacks found in human transcriptomic studies, because studies on AD examining brain tissue have produced largely discordant results (26). Human transcriptomic data suffer from serious noise because of tissue quality and variation in the agonal state of the patients. These problems can be circumvented in mice by isolating high-quality RNA from animals reared and then killed in highly controlled conditions. Additionally, transcriptomics studies comparing disease and control conditions identify not only causative genes but also, secondarily affected genes. To focus on causative genes, we determined the strain effects on gene expression profiles before the Aβ analysis in *APP*-Tg mice. Using non-Tg mice in the absence of Aβ pathology enabled us to select the genes with expression levels that were changed by the genetic background but not the Aβ pathology (Fig. 3*A*, second selection step). Finally, using Tg mice with mixed genetic backgrounds, we confirmed that Aβ levels were negatively dependent on the number of DBA alleles in the *Klc1* regions (Fig. 3*B*, *Right*). DNA sequence variation as causative in disease has also been implicated in other studies (27–29). In summary, the strengths of each approach (model mice with mixed genetic backgrounds and transcriptomics) are synergized, whereas their respective drawbacks are minimized.

Kinesin-1 is a plus end-directed motor comprised of two kinesin heavy chains and two KLCs that associate in a 1:1 stoichiometry (30). KLC1, with expression that is enriched in neuronal tissue (31), is required for cargo binding and the regulation of motility. Among myosin and kinesin family members, splicing is a common strategy to facilitate motor cargo selection, and the many splice variants of KLC1 in the C-terminal region likely allow it to select different cargos (32). Notably, all *KLC1* splice variants discovered thus far share extensive similarity between human, mouse, and rat (Fig. S7) (24), suggesting an essential role for each variant. The importance of splicing of *KLC1*, however, has been relatively ignored; in most *KLC1* studies, all variants of *KLC1* have been abolished, or the single major isoform has been overexpressed. In a mouse model that knocks out one allele of the *Klc1* gene, an increase in Aβ was seen (33), whereas knocking down *KLC1* in stem cells decreased Aβ (34). These seemingly conflicting results could be explained by splicing of *KLC1*. The transport of APP requires KLC1 to act as a direct or indirect motor cargo adaptor (35–40), and changes in the splicing of *KLC1* may alter such interactions. Additional studies are required to fully understand the mechanistic role of KLC1 in AD.

Disruption of trafficking is usually thought to be a result of Aβ pathology. However, the present study and several other studies (33–36, 38, 39, 41) show just the opposite, where alterations in trafficking can modify Aβ pathology. Moreover, recent genome-wide association studies identified trafficking-related genes (*PICALM*, *BIN1*, *CD33*, and *CD2AP*) as AD risk genes (42), further suggesting that trafficking is a causative factor of AD.

In conclusion, *Klc1* variant E was identified as an Aβ modifier using a hypothesis-free transcriptomics approach. Notably, common interstrain genetic variations (polymorphisms) affected the expression levels of *Klc1* variant E and modified Aβ accumulation in mice. Subsequently, a corresponding variation in the expression levels of *KLC1* variant E in sporadic AD in the human population was discovered. These findings, along with other studies (33–39, 41), add a critical element to the understanding of AD etiology and implicate intracellular trafficking as a causative factor in Aβ accumulation. The present study also shows that the combination of animal models and transcriptomics is an effective strategy for identifying unique genes causative in complex human diseases.

Materials and Methods

Animals. We crossed Tg2576 mice with a genetic background of 50% B6 and 50% SJL onto three inbred strains (B6, SJL, and DBA) for one to three

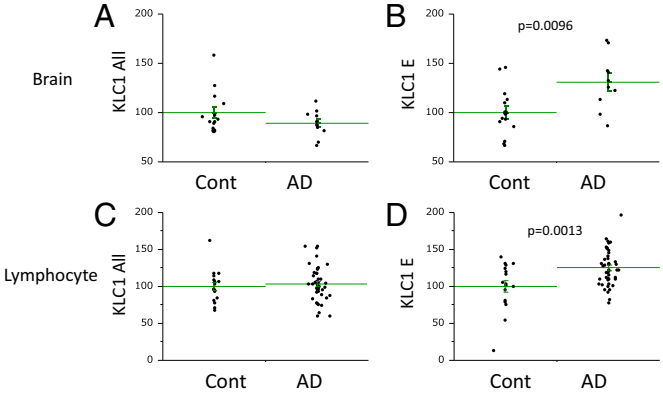

Fig. 5. Levels of total *KLC1* and *KLC1* variant E in humans. Brain expression levels of (*A*) *KLC1* All and (*B*) *KLC1* E were measured in control ($n = 14$) and AD ($n = 10$) patients by QPCR. Lymphocyte expression levels of (*C*) *KLC1* All and (*D*) *KLC1* E were also measured in control ($n = 17$) and AD ($n = 47$) patients. Long and short green bars indicate mean and SE, respectively. The mean expression levels of the control were normalized to 100.

generations and intercrossed the offspring. As a result, six groups of *APP*-Tg mice with different percentages of background genomes from B6, SJL, and DBA were generated (Fig. 1*A*). In the first *APP*-Tg mouse group ($n = 16$), 62.5% of the genome randomly came from B6, and 37.5% of the genome randomly came from SJL, which was expected. In the second group ($n = 14$), mice had a mixture of 84% SJL and 16% B6. In the third group ($n = 10$), mice had 69% SJL and 31% B6. In the fourth group ($n = 8$), mice had 50% DBA, 31% B6, and 19% SJL. In the fifth group ($n = 3$), mice had 50% DBA, 42% SJL, and 8% B6. In the sixth group ($n = 8$), mice had 75% DBA, 16% B6, and 9% SJL.

To minimize variance in the animal samples, all animals were killed at 10:00 AM at the age of 12 (or 6) mo, and they were killed within 1 wk of each another. Animals were perfused before brain dissection with 15–20 mL 0.05 M tris-buffered saline (pH 7.2–7.4) containing a Protease Inhibitor Mixture (P2714; Sigma). The hippocampus, frontal region, residual cortex, and cerebellum were dissected out and snap-frozen in liquid nitrogen (43). All animal procedures were performed according to the protocols approved by the Osaka University Animal Care and Use Committee.

Human Brain. Brains were obtained from the brain bank of the Choju Medical Institute of Fukushimura Hospital. We examined the hippocampi of 27 patients. Three poor-quality samples with RNA integrity numbers, determined by the 2100 Bioanalyzer (Agilent), that were under seven were excluded from the analysis. All brains, including brains excluded from the analysis, received a pathological diagnosis (AD: $n = 10$, control: $n = 14$) (Table S2). AD diagnosis was according to the criteria of the Consortium to Establish a Registry for Alzheimer's Disease and Braak Stage. Control patients had died without dementia. The protocol used was approved independently by the local ethics committees of Osaka University and Fukushimura Hospital.

Human Blood Samples. The AD cases were recruited from Osaka University Hospital (44, 45) and met the criteria of the National Institute of Neurological and Communicative Disorders and Stroke and the Alzheimer's Disease and Related Disorders Association criteria for probable AD. The control cases were recruited from healthy elderly volunteers with no history of dementia or other neuropsychiatric diseases (44, 45). The purpose and significance of the present study were explained in detail to each patient and his/her family, and all subjects provided their informed consent. The protocol for specimen collection was approved by the genome ethical committee of Osaka University Graduate School of Medicine. DNA was extracted from white blood nuclear cells using the QIAmp DNA Blood Maxi Kit (QIAGEN). RNA was extracted using a Paxgene tube (QIAGEN) following the manufacturer's protocol.

Additional information regarding Aβ measurements, Western blotting, expression arrays, QPCR, genotyping, cell cultures, reanalysis of two other studies using a mouse phenome database, and statistical analysis is in *SI Materials and Methods*.

ACKNOWLEDGMENTS. We thank Mitsuko Yamamoto, Noriko Kuwabara, and Kiyoko Kato for carrying out and assisting with experiments. This work was supported by KAKENHI (C) Grant-in-Aid for Scientific Research 23591706 (to T.M.), The Sakamoto Research Institute of Psychopathology (T.M.), a Health Labour Sciences Research Grant (to T.M. and M.T.) from the Ministry of Health Labour and Welfare of Japan, the Japanese Brain Bank Network for Neuroscience Research (to H.A.) and Integrated Research on Neuropsychiatric Disorders carried out under the Strategic Research Program for Brain Sciences (to M.T.) under the Ministry of Education, Culture, Sports, Science, and Technology of Japan, and a KAKENHI Grant on Priority Areas Applied Genomics (to M.T.). M.A.S. thanks the Japanese Society for Promotion of Science for Long-Term Invitation Fellowship ID L11710 and Dr. Y. Yoneda for support.

1. Bertram L, McQueen MB, Mullin K, Blacker D, Tanzi RE (2007) Systematic meta-analyses of Alzheimer disease genetic association studies: The AlzGene database. *Nat Genet* 39(1):17–23.
2. Naj AC, et al. (2011) Common variants at MS4A4/MS4A6E, CD2AP, CD33 and EPHA1 are associated with late-onset Alzheimer's disease. *Nat Genet* 43(5):436–441.
3. Hollingworth P, et al. (2011) Common variants at ABCA7, MS4A6A/MS4A4E, EPHA1, CD33 and CD2AP are associated with Alzheimer's disease. *Nat Genet* 43(5):429–435.
4. Seshadri S, et al. (2010) Genome-wide analysis of genetic loci associated with Alzheimer disease. *JAMA* 303(18):1832–1840.
5. Harold D, et al. (2009) Genome-wide association study identifies variants at CLU and PICALM associated with Alzheimer's disease. *Nat Genet* 41(10):1088–1093.
6. Lambert J-C, et al. (2009) Genome-wide association study identifies variants at CLU and CR1 associated with Alzheimer's disease. *Nat Genet* 41(10):1094–1099.
7. Jonsson T, et al. (2013) Variant of TREM2 associated with the risk of Alzheimer's disease. *N Engl J Med* 368(2):107–116.
8. Guerreiro R, et al. (2013) TREM2 variants in Alzheimer's disease. *N Engl J Med* 368(2): 117–127.
9. Gatz M, et al. (2006) Role of genes and environments for explaining Alzheimer disease. *Arch Gen Psychiatry* 63(2):168–174.
10. Holton P, et al. (2013) Initial assessment of the pathogenic mechanisms of the recently identified Alzheimer risk Loci. *Ann Hum Genet* 77(2):85–105.
11. Bertram L, Tanzi RE (2009) Genome-wide association studies in Alzheimer's disease. *Hum Mol Genet* 18(R2):R137–R145.
12. Antonarakis SE, Chakravarti A, Cohen JC, Hardy J (2010) Mendelian disorders and multifactorial traits: The big divide or one for all? *Nat Rev Genet* 11(5):380–384.
13. Pedersen NL (2010) Reaching the limits of genome-wide significance in Alzheimer disease: Back to the environment. *JAMA* 303(18):1864–1865.
14. Flint J, Eskin E (2012) Genome-wide association studies in mice. *Nat Rev Genet* 13(11): 807–817.
15. Flint J, Valdar W, Shifman S, Mott R (2005) Strategies for mapping and cloning quantitative trait genes in rodents. *Nat Rev Genet* 6(4):271–286.
16. Womack JE, Jang H-J, Lee MO (2012) Genomics of complex traits. *Ann N Y Acad Sci* 1271:33–36.
17. Bras J, Guerreiro R, Hardy J (2012) Use of next-generation sequencing and other whole-genome strategies to dissect neurological disease. *Nat Rev Neurosci* 13(7):453–464.
18. Ryman D, Gao Y, Lamb BT (2008) Genetic loci modulating amyloid-beta levels in a mouse model of Alzheimer's disease. *Neurobiol Aging* 29(8):1190–1198.
19. Sebastiani G, et al. (2006) Mapping genetic modulators of amyloid plaque deposition in TgCRND8 transgenic mice. *Hum Mol Genet* 15(15):2313–2323.
20. Sullivan PF, Fan C, Perou CM (2006) Evaluating the comparability of gene expression in blood and brain. *Am J Med Genet B Neuropsychiatr Genet* 141B(3):261–268.
21. Lehman EJH, et al. (2003) Genetic background regulates beta-amyloid precursor protein processing and beta-amyloid deposition in the mouse. *Hum Mol Genet* 12(22):2949–2956.
22. Grubb SC, Maddatu TP, Bult CJ, Bogue MA (2009) Mouse phenome database. *Nucleic Acids Res* 37(Database Issue):D720–D730.
23. Petkov PM, et al. (2004) An efficient SNP system for mouse genome scanning and elucidating strain relationships. *Genome Res* 14(9):1806–1811.
24. McCart AE, Mahony D, Rothnagel JA (2003) Alternatively spliced products of the human kinesin light chain 1 (KNS2) gene. *Traffic* 4(8):576–580.
25. Webster JA, et al. (2009) Genetic control of human brain transcript expression in Alzheimer disease. *Am J Hum Genet* 84(4):445–458.
26. Sutherland GT, Janitz M, Kril JJ (2011) Understanding the pathogenesis of Alzheimer's disease: Will RNA-Seq realize the promise of transcriptomics? *J Neurochem* 116(6):937–946.
27. Lee Y, et al. (2012) Variants affecting exon skipping contribute to complex traits. *PLoS Genet* 8(10):e1002998.
28. Emilsson V, et al. (2008) Genetics of gene expression and its effect on disease. *Nature* 452(7186):423–428.
29. Chen Y, et al. (2008) Variations in DNA elucidate molecular networks that cause disease. *Nature* 452(7186):429–435.
30. Hirokawa N (1998) Kinesin and dynein superfamily proteins and the mechanism of organelle transport. *Science* 279(5350):519–526.
31. Rahman A, Kamal A, Roberts EA, Goldstein LSB (1999) Defective kinesin heavy chain behavior in mouse kinesin light chain mutants. *J Cell Biol* 146(6):1277–1288.
32. Woźniak MJ, Allan VJ (2006) Cargo selection by specific kinesin light chain 1 isoforms. *EMBO J* 25(23):5457–5468.
33. Stokin GB, et al. (2005) Axonopathy and transport deficits early in the pathogenesis of Alzheimer's disease. *Science* 307(5713):1282–1288.
34. Killian RL, Flippin JD, Herrera CM, Almenar-Queralt A, Goldstein LSB (2012) Kinesin light chain 1 suppression impairs human embryonic stem cell neural differentiation and amyloid precursor protein metabolism. *PLoS One* 7(1):e29755.
35. Kamal A, Stokin GB, Yang Z, Xia CH, Goldstein LS (2000) Axonal transport of amyloid precursor protein is mediated by direct binding to the kinesin light chain subunit of kinesin-I. *Neuron* 28(2):449–459.
36. Kamal A, Almenar-Queralt A, LeBlanc JF, Roberts EA, Goldstein LS (2001) Kinesin-mediated axonal transport of a membrane compartment containing beta-secretase and presenilin-1 requires APP. *Nature* 414(6864):643–648.
37. Lazarov O, et al. (2005) Axonal transport, amyloid precursor protein, kinesin-1, and the processing apparatus: Revisited. *J Neurosci* 25(9):2386–2395.
38. Araki Y, et al. (2007) The novel cargo Alcadein induces vesicle association of kinesin-1 motor components and activates axonal transport. *EMBO J* 26(6):1475–1486.
39. Vagnoni A, et al. (2012) Calsyntenin-1 mediates axonal transport of the amyloid precursor protein and regulates Aβ production. *Hum Mol Genet* 21(13):2845–2854.
40. Goldstein LSB (2012) Axonal transport and neurodegenerative disease: Can we see the elephant? *Prog Neurobiol* 99(3):186–190.
41. Muresan V, Muresan Z (2012) A persistent stress response to impeded axonal transport leads to accumulation of amyloid-β in the endoplasmic reticulum, and is a probable cause of sporadic Alzheimer's disease. *Neurodegener Dis* 10(1–4):60–63.
42. Bettens K, Sleegers K, Van Broeckhoven C (2013) Genetic insights in Alzheimer's disease. *Lancet Neurol* 12(1):92–104.
43. Lim GP, et al. (2005) A diet enriched with the omega-3 fatty acid docosahexaenoic acid reduces amyloid burden in an aged Alzheimer mouse model. *J Neurosci* 25(12):3032–3040.
44. Kimura R, et al. (2007) The DYRK1A gene, encoded in chromosome 21 Down syndrome critical region, bridges between beta-amyloid production and tau phosphorylation in Alzheimer disease. *Hum Mol Genet* 16(1):15–23.
45. Hayashi N, et al. (2010) KIBRA genetic polymorphism influences episodic memory in Alzheimer's disease, but does not show association with disease in a Japanese cohort. *Dement Geriatr Cogn Disord* 30(4):302–308.

Supporting Information

Morihara et al. 10.1073/pnas.1307345111

SI Materials and Methods

Amyloid-β Measurements in Mouse Brain. Amyloid-β (Aβ) measurements were performed in the remaining cortical samples as previously described (1). Using a BioPulverizer (BioSpec Product), samples were powdered and divided into two tubes. Because our preliminary experiments showed that the largest contributor to technical variance was at the homogenization step, we performed two independent homogenizations of powdered tissue at different times and measured Aβ levels in the two independently homogenized samples.

Brain samples were homogenized with five wet weight volumes of 1% Triton-X and 25 mM tris-buffered saline (TBS) (pH 7.9) with Complete Protease Inhibitor Mixture (Roche). After sitting on ice for 3 h, the homogenized samples were centrifuged at 100,000 × *g* for 20 min at 4 °C. The supernatants were used for Aβ ELISAs. The pellets were mixed with five wet weight volumes of 5 M guanidine HCl and sonicated at room temperature. After rotation for 2 h at room temperature, the mixtures were diluted with TBS and centrifuged at 4,000 × *g* for 20 min at 4 °C. The supernatants were neutralized before loading onto the ELISAs plates. Aβ levels were measured by ELISA following the manufacturer's protocol (Wako).

APP Western Blotting. Powdered brain samples were homogenized with 10 wet weight volumes of 1% Nonidet P-40, 10 mM Tris·HCl (pH 7.8), 150 mM NaCl, and 1 mM EDTA lysis buffer. Western blotting was performed using 22C11 antibody (NAB384; Chemicon).

Expression Array. The quality of RNA was assessed for each sample using an Agilent 2100 Bioanalyzer (Agilent Technologies). Forty RNA samples were analyzed by the Illumina Mouse Ref-8 Expression BeadChip (Illumina) using standard protocols. All expression profiles were extracted and rank invariant-normalized using BeadStudio software (Illumina). The levels of Aβ were transformed into log form and analyzed further using GeneSpring GX, version 10 (Agilent Technology) and JMP 9 (SAS Institute).

Quantitative PCR Primers and Probes. The ABI predesigned quantitative PCR (QPCR) assay (Mm00492936_m1) with primers located in exons 3 and 4 was used to detect all splice forms of kinesin light chain-1 (*Klc1*). Using Primer Express (Applied Biosystems), splice form-specific QPCR assays were designed as described previously (2). Each reverse primer was designed on the exon boundaries specific to each splice form. Absence of SNPs in these primers was verified by Ensemble (www.ensembl.org). The specific amplification of these primers was confirmed as follows: first, in silico analysis using Primer-Blast (www.ncbi.nlm.nih.gov/tools/primer-blast/index.cgi?LINK_LOC=BlastHome); second, assessment of the dissociation curve of the amplicons; also, in some cases, gel electrophoresis of the amplicons and/or the absence of amplification with mismatched splice forms. The forward primer common for *Klc1* variants A–E specific assays was GTCTCAATATGGACGTGGTCAAGTA, and the TaqMan MGB probe common for each splice specific assay was TCCGTCAGGGCCACT. The reverse primers were Klc1A: GGGCGGCTAGGCTTCCT; Klc1B: CCCGAGCTTCATCTTTCTCATTT; Klc1C: CATCCCATTCCACTCTACGC; Klc1D: GCCATCCCCATTCCACTCTA; and Klc1E: GATCCAGTGCCATCTTCCTCC. QPCR assays for all splice forms of *KLC1* and specific assays for each splice forms were also designed. The forward primer common for each *KLC1* assay was TCTCGTAAACAGGGTCTTGACAATG. The TaqMan MGB probe common for each *Klc1* assay was ATGACCCTGAGAACAT. The reverse primer detecting all splice forms of *KLC1* was GGCCACTCTCGTACTTGACCAC, and the reverse primer for KLC1E was TGCCATCTTCCTCCCCTCC. For endogenous control assays, we used TaqMan Gene Expression Assays (Endogenous Control). The assay identifications were Hs99999905_m1 for *GAPDH*, *HPRT1* Hs99999909_m1 for *HPRT1*, Hs99999901_s1 for human and mouse *18S*, and Mm00446968_m1 for *Hprt1*.

Genotyping. Genotyping of *Klc1* (rs6390948, rs13481650, rs13481653, and rs13481656) and *APOE* polymorphisms was performed by the TaqMan SNP assay and ABI Prism 7900HT sequence detection system (Applied Biosystems) as previously described (3, 4).

Cell Culture. pFLC1 Vector-Mouse Klc1-D cDNA was purchased from DNAFORM. mKlc1-D cDNA encoding 615 aa (GenBank accession no. NM1025360.2) was subcloned into a pcDNA3.1(-) vector (Invitrogen) at the EcoR1/BamH1 sites to produce pcDNA3.1(-)-mKlc1-D. pcDNA3.1(-)-mKlc1 D had 27 bases deleted from 1819 to 1845 using the QuikChange site-directed mutagenesis kit (Stratagene) to produce pcDNA3.1(-)-mKlc1-E. The primers for mutagenesis were TGACGGAGGGGAGGAAGATGGCACTGGATCTT (sense) and AAGATCCAGTGCCATCTTCCTCCCCTCCGTCA (antisense). The expression of *Klc1* variant E was confirmed by Western blotting using antibody UT109 (1:500) (5).

A neuronal cell line (mouse neuroblastoma Neuro2A cells) was cultured in DMEM with 10% (vol/vol) FCS. One day before transfection, cells were plated at 1.5×10^4 cells/cm^2 onto six-well plates coated with 0.01% poly-L-lysine (Wako). N2a cells were transfected with *Klc1* variant E or empty plasmid using HilyMax (Dojindo) according to the manufacturer's protocol ($n = 11$ per group). The medium was changed after 6 h; 72 h after transfection, medium was collected and centrifuged at 70 × *g* for 1 min. Aβ levels in the supernatant was measured by ELISA [Human/RatβAmyloid(40) ELISA Kit, Catalog 294–62501 and Human/Rat βAmyloid(42) ELISA Kit, Catalog 290–62601; Wako].

Using BLOCK-iT RNAi Designer (Invitrogen), we developed *KLC1* variant E Stealth siRNA (*KLC1* E siRNA), which was designed for the exon boundary specific to *KLC1* splice variant E, *KLC1* ALL Stealth siRNA (*KLC1* All siRNA), which was designed for the common exon for all splice variants, and custom scrambled Stealth siRNAs for *KLC1* E or *KLC1* All. The siRNA sequences were *KLC1* E siRNA: GAGGAAGAUGGCACUGGAUCUUUAA; *KLC1* E control: GAGGAUAGGACUCGGUAUCUAGUAA; *KLC1* All siRNA: UCCGGAUCAUGUUUGAUUUCUCCUC; and *KLC1* All control: GAGAAAGAACUUACACUAGCAGGGA.

Neuronal cell line stably expressing APPsw (human neuroblastoma SH-SY5Y) was cultured in DMEM/F12 (1:1; Gibco) with 5% FCS. One day before transfection, cells were plated at 2.0×10^5 cells/dish onto 6-cm plates; 2.7 (KLC1 E siRNA and KLC1 E control) or 27 pmol siRNA (KLC1 ALL siRNA and KLC1 ALL control) were mixed with 10 μL Lipofectamine RNAiMAX (Invitrogen) in 1 mL Opti-MEM Reduced Serum Medium (Gibco). The mixture was added to the cells in 5 mL culture medium without antibiotics; 72 h after transfection, medium was collected, and RNA was isolated (RNeasy Mini Kit; Qiagen). Aβ levels in the medium were measured by ELISA. The levels of mRNA were measured by QPCR as described above.

Reanalysis of Two Other *APP*-Tg Mice Studies and a Mouse Phenome Database. Two groups have reported genomic regions that may control Aβ accumulation in mice (6–8). The genomic regions,

however, did not coincide, and the reports did not identify the region containing *Klc1*. In contrast to the discordant results of the gene screening, the phenotype of Aβ accumulation in each mouse strain was consistent between those reports and the present one (Fig. S4). To reexamine the association between the *Klc1* allele and Aβ accumulation using the results from these two studies and our data, we searched the mouse phenome database (www.jax.org/phenome) (9) and obtained SNPs data. In the mouse phenome database, the CGD1 dataset was selected and thresholded for confidence levels on imputed calls set at 0.9 (default). Genomic region chromosome 12 (11.995674–113.039450 Mbp; Build 37) was selected as the *Klc1* region. The search was performed on August 22, 2011.

Statistical Analysis. The statistics for array expression analysis are described above and in *Results*, *Mouse Transcriptomics Identify Klc1 as a Modifier of Aβ Accumulation*. Other statistical analyses were performed using JMP 9 (SAS Institute). Unless otherwise specified, a two-sided *P* value less than 0.05 was considered significant.

1. Lim GP, et al. (2005) A diet enriched with the omega-3 fatty acid docosahexaenoic acid reduces amyloid burden in an aged Alzheimer mouse model. *J Neurosci* 25(12): 3032–3040.
2. Morihara T, et al. (2005) Ibuprofen suppresses interleukin-1beta induction of pro-amyloidogenic alpha1-antichymotrypsin to ameliorate beta-amyloid (Abeta) pathology in Alzheimer's models. *Neuropsychopharmacology* 30(6):1111–1120.
3. Kimura R, et al. (2007) The DYRK1A gene, encoded in chromosome 21 Down syndrome critical region, bridges between beta-amyloid production and tau phosphorylation in Alzheimer disease. *Hum Mol Genet* 16(1):15–23.
4. Hayashi N, et al. (2010) KIBRA genetic polymorphism influences episodic memory in Alzheimer's disease, but does not show association with disease in a Japanese cohort. *Dement Geriatr Cogn Disord* 30(4):302–308.
5. Araki Y, et al. (2007) The novel cargo Alcadein induces vesicle association of kinesin-1 motor components and activates axonal transport. *EMBO J* 26(6):1475–1486.
6. Ryman D, Gao Y, Lamb BT (2008) Genetic loci modulating amyloid-beta levels in a mouse model of Alzheimer's disease. *Neurobiol Aging* 29(8):1190–1198.
7. Sebastiani G, et al. (2006) Mapping genetic modulators of amyloid plaque deposition in TgCRND8 transgenic mice. *Hum Mol Genet* 15(15):2313–2323.
8. Lehman EJH, et al. (2003) Genetic background regulates beta-amyloid precursor protein processing and beta-amyloid deposition in the mouse. *Hum Mol Genet* 12(22): 2949–2956.
9. Grubb SC, Maddatu TP, Bult CJ, Bogue MA (2009) Mouse phenome database. *Nucleic Acids Res* 37(Database Issue):D720–D730.

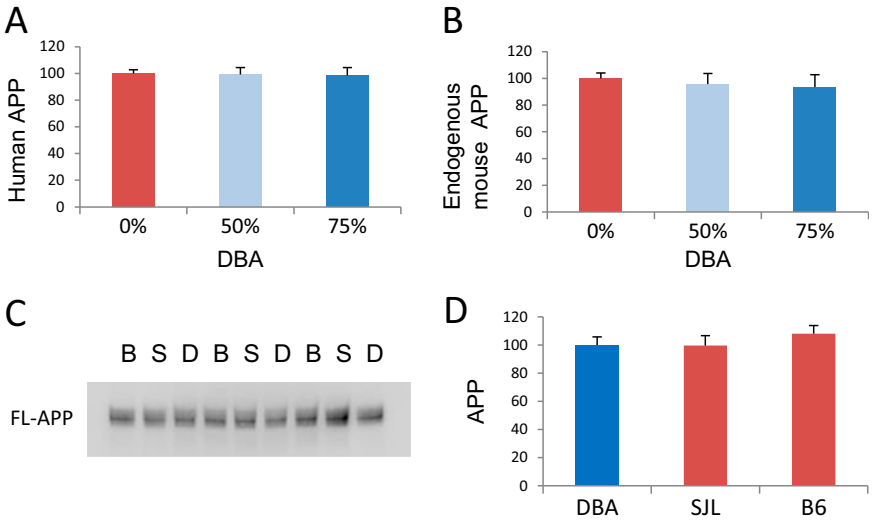

Fig. S1. Levels of APP in mouse brain. mRNA levels of (*A*) transgene human and (*B*) endogenous mouse *APP* in *APP*-Tg mice carrying no DBA/2 (DBA), 50% DBA, and 75% DBA genetic background as measured by QPCR. No effect on the levels of *APP* mRNA expression by the amount of DBA genetic background was observed. Levels in mice with no DBA genetic background were normalized to 100. (*C*) Western blotting of inbred (non-Tg) mouse strains. Brain full length APP (FL-APP) protein levels in C57BL/6 (B), SJL (S), and DBA/2 (D) strains are shown. (*D*) APP protein levels in the three strains using semiquantitative analysis of the Western blots. B6, C57BL/6. No significant differences between strains were observed. Levels in DBA inbred mice were normalized to 100. Error bars indicate SEM. These data suggested that the regulation of APP expression levels was not involved in the mechanism of Aβ suppression by the DBA genetic background.

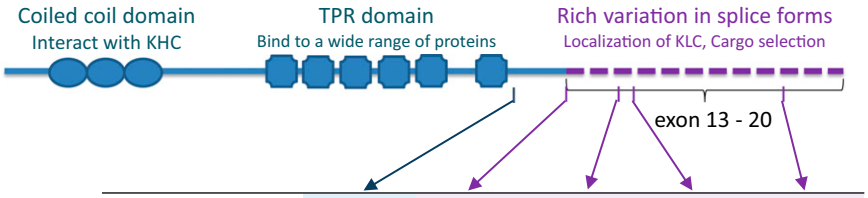

Probe ID	7330358	4050133	540139	6130468	4060520
Probe location	Common region of all splice forms	Alternative splice region			
Genome-wide screening (Fig. 2)		✓		✓	
DBA<B6 p value[a] in non-Tg mice	0.91	<0.0001	<0.0001	<0.0001	<0.0001
DBA<SJL p value[a] in non-Tg mice	0.30	<0.0001	<0.0001	<0.0001	<0.0001
Correlation with Aβ p value[b] in *APP*-Tg mice	0.49	Positive p<0.0001	Positive p<0.0001	Positive p<0.0001	Positive p<0.0001

Fig. S2. Locations and expression patterns of all probes in *Klc1*. Illumina mouse Ref-8 Expression BeadChip has five probes in *Klc1*. The signal levels of probe 7330358, which is located in a common region for all splice forms, were not different between DBA and the other inbred strains. Also, it did not correlate with Aβ levels in *APP*-Tg mice with mixed genetic backgrounds. The signal levels of 4050133, 540139, 6130468, and 4060520 were lower in DBA compared with those levels in B6 or SJL and positively correlated with the Aβ levels in *APP*-Tg mice. All four probes were located in the splice region of *Klc1*. [a]Unpaired *t* test without multiple testing correction. [b]Pearson product moment correlation. TPR, tetratricopeptide repeat.

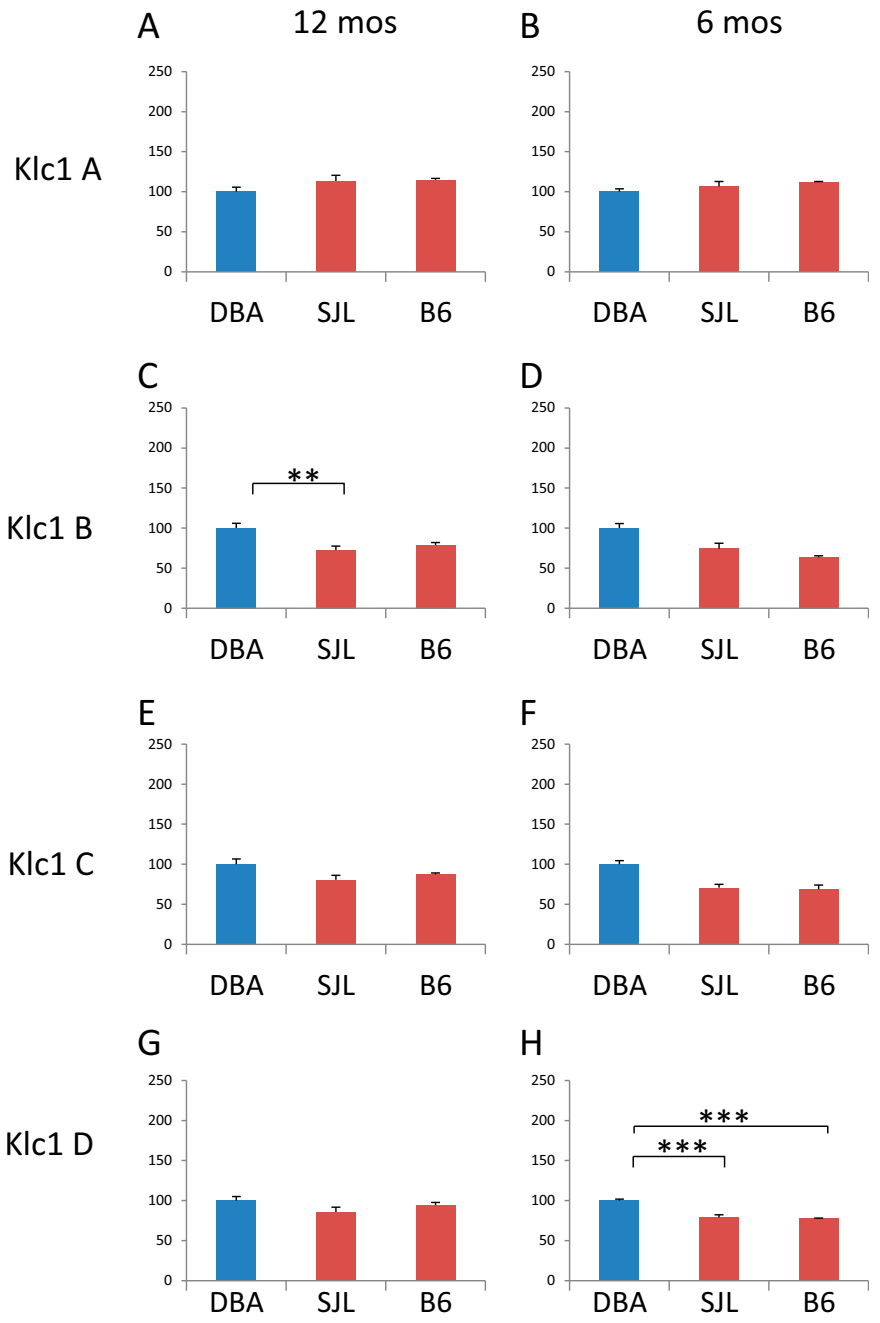

Fig. S3. Expression levels of *Klc1* variants A–D in the three strains (non-Tg mice). mRNA expression levels of *Klc1* variants (*A* and *B*) A, (*C* and *D*) B, (*E* and *F*) C, and (*G* and *H*) D in non-Tg mice at (*A*, *C*, *E*, and *G*) 12 [$n = 7$ (DBA), 6 (SJL), and 7 (B6)] and (*B*, *D*, *F*, and *H*) 6 mo of age [$n = 4$ (DBA), 4 (SJL), and 3 (B6)] were measured by QPCR. *P* values were calculated by the Tukey–Kramer Honestly Significant Difference test and considered significant when less than 0.004 (0.05/12 tests) according to Bonferroni correction for multiple testing. $^{**}P < 0.01$; $^{***}P < 0.001$. The expression levels in DBA were set to 100. Error bars indicate SEM.

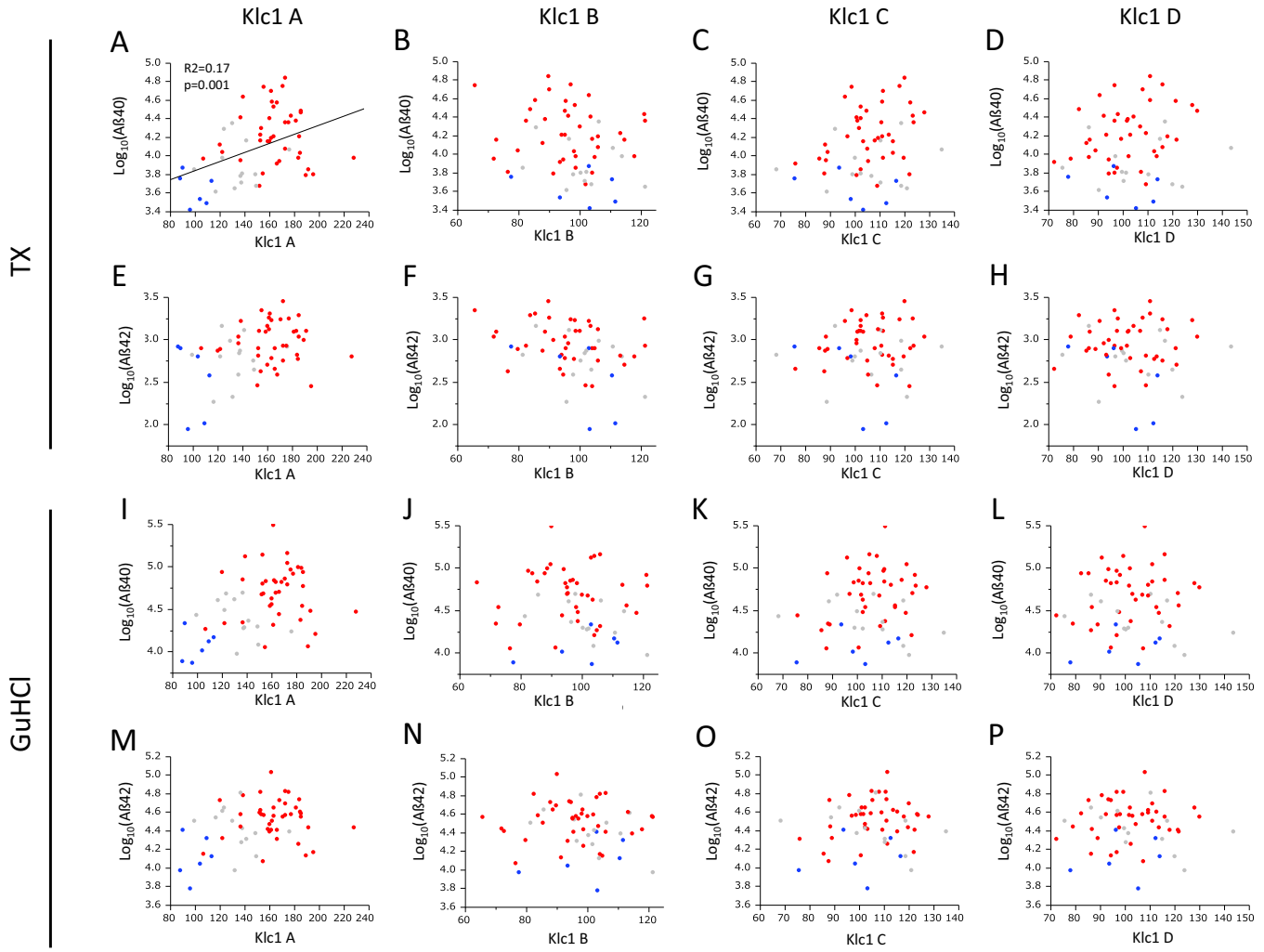

Fig. S4. Relationship between levels of Aβ accumulation and *Klc1* expression and number of *Klc1* alleles from DBA in *APP*-Tg mice with mixed genetic backgrounds. Expression levels of (*A*, *E*, *I*, and *M*) *Klc1* variant A, (*B*, *F*, *J*, and *N*) *Klc1* variant B, (*C*, *G*, *K*, and *O*) *Klc1* variant C, and (*D*, *H*, *L*, and *P*) *Klc1* variant D in *APP*-Tg mice with mixed genetic backgrounds ($n = 59$) are shown on the *x* axis. (*A*–*D*) Aβ40 and (*E*–*H*) Aβ42 levels in Triton-X (TX) fractions and (*I*–*L*) Aβ40 and (*M*–*P*) Aβ42 levels in guanidine HCl (GuHCl) fractions in mouse brain are shown in log10 scale on the *y* axis (picograms Aβ per milligram total protein). Lines show the correlation between the levels of *Klc1* and Aβ. *P* values are considered significant when they are less than 0.002 (0.05/24 tests) according to Bonferroni correction for multiple testing. Blue, mice carrying two *Klc1* alleles from DBA strain; gray, mice carrying one Klc1 allele from DBA; red, mice carrying no *Klc1* allele from DBA. Mean expression levels in mice carrying two DBA alleles were normalized to 100.

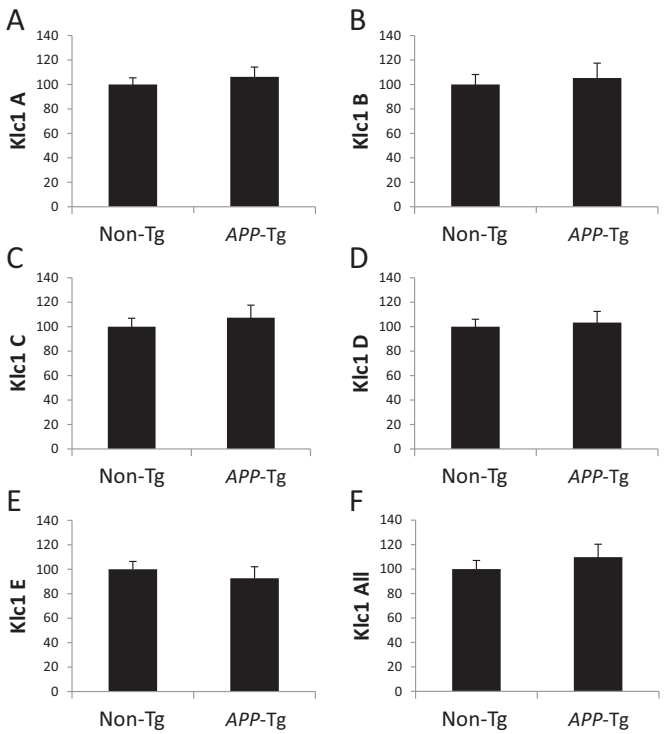

Fig. S5. Brain expression levels of *Klc1* splice variants and total *Klc1* in non-Tg and *APP*-Tg mice. Expression levels of (*A*–*E*) *Klc1* splice variants and (*F*) total *Klc1* in non-Tg ($n = 9$) and *APP*-Tg mice ($n = 4$) littermates at 12 mo of age were measured by QPCR. (*E*) The mRNA levels of *Klc1* variant E were not elevated in *APP*-Tg mice (−7.44%, $P = 0.52$; Student *t* test) compared with those levels in non-Tg littermates. The expression levels of (*A*–*D*) the other splice variants of *Klc1* and (*F*) total levels of *Klc1* (*Klc1* All) were also similar between *APP*-Tg and non-Tg mice. These data show that Aβ did not affect the overall expression levels of *Klc1* in any form, strengthening the evidence that the correlation between *Klc1* variant E and Aβ in *APP*-Tg mice (Fig. 3*B*, *Right*) was unlikely caused by Aβ accumulation. Levels of non-Tg mice were normalized to 100. Error bars indicate SEM.

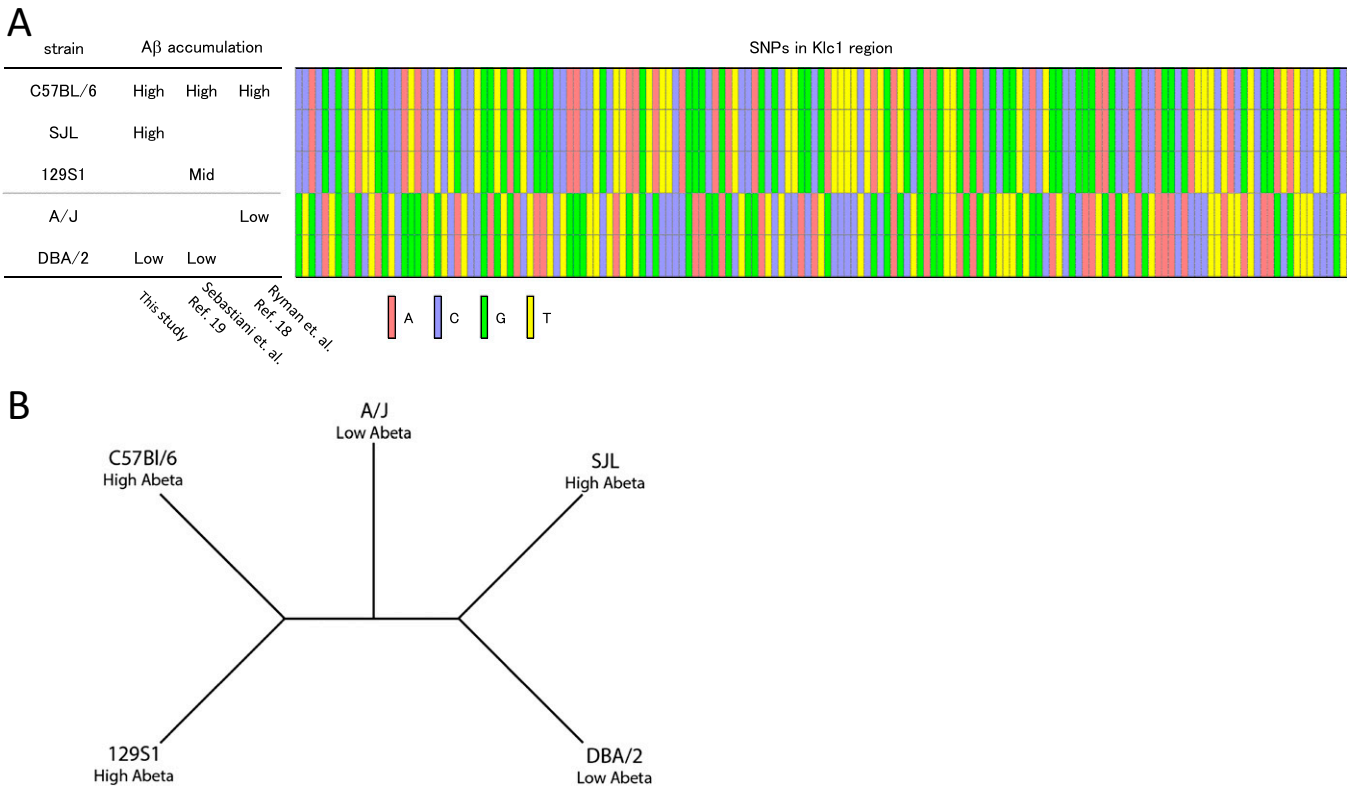

Fig. S6. Aβ high and low mouse strains. (*A*) *Klc1* alleles in high and low Aβ mouse strains. Relative Aβ accumulations in each mouse strain are shown in *Left*; 159 SNPs (color bars) in the *Klc1* region (chromosome 12: 112.995674–113.039450 Mbp; Build 37) of C57BL/6, SJL, 129S1, A/J, and DBA/2 mice are shown in *Right*. SNPs data were obtained from the Jax mouse phenome database (http://phenome.jax.org). (*B*) Unrooted relationships of the five mouse strains indicating independent evolution of *Klc1*. Modified from ref. 1.

1. Petkov PM, et al. (2004) An efficient SNP system for mouse genome scanning and elucidating strain relationships. *Genome Res* 14(9):1806–1811.

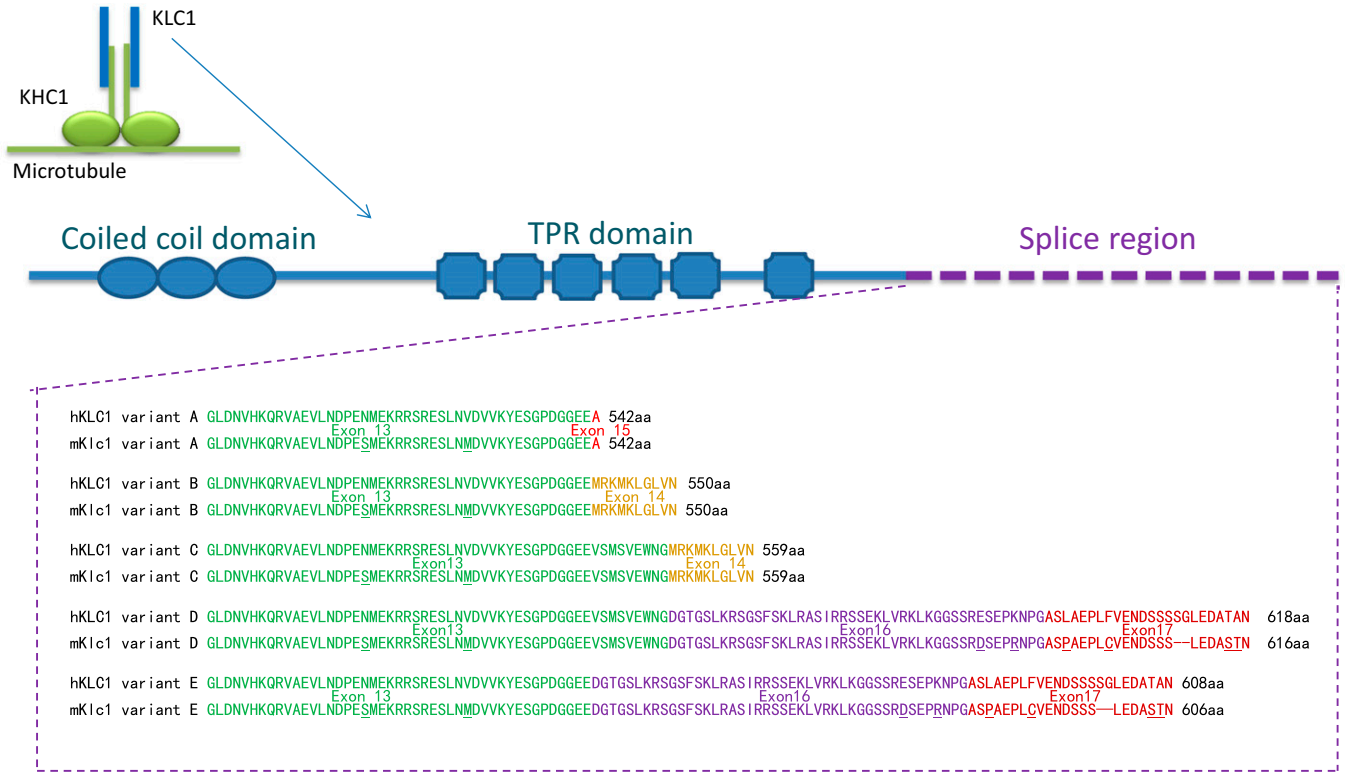

Fig. S7. Highly conserved alternatively splicing of KLC1 between human and mice. The amino acid sequences of human KLC1 (hKLC1) and mouse Klc1 (mKlc1) are highly conserved (variant A, 94.5%; variant B, 94.4%; variant C, 94.5%; variant D, 93.1%; variant E, 93.6%). Mouse residues that differ from human sequences are underlined. Gaps (—) have been included to facilitate alignment. (*Upper*) Exons 1–12 (residues 1–496) are common for all splice variants of KLC1 and include coiled coil and tetratricopeptide repeat (TPR) domains. (*Lower*) Exon 13 and its following exons (C termini of KLC1) are different among splice variants. Modified from ref. 1.

1. McCart AE, Mahony D, Rothnagel JA (2003) Alternatively spliced products of the human kinesin light chain 1 (KNS2) gene. *Traffic* 4(8):576–580.

Table S1. Fifty-four probes with lower or higher signal in DBA strains

Gene name	Gene symbol	Gene ID	Illumina probe ID	Fold change (DBA vs. B6)	Fold change (DBA vs. SJL)
Lower					
Activating transcription factor 4	*Atf4*	11911	2480692	34.65	33.61
ADP ribosylation factor GTPase activating protein 2	*Arfgap2*	77038	5220678	3.23	3.60
Amyloid-β precursor protein (cytoplasmic tail) binding protein 2	*Appbp2*	66884	1240564	1.82	1.88
Ataxin 1	*Atxn1*	20238	2450187	2.84	2.99
Basic helix–loop–helix domain containing, class B2	*Bhlhb2*	20893	1230341	16.73	13.64
Coiled-coil domain containing 88A	*Ccdc88a*	108686	3400440	7.63	7.61
Coiled-coil domain containing 53	*Ccdc53*	67282	6380059	7.31	7.04
Death-associated protein 3	*Dap3*	65111	6100014	2.03	1.79
Death-associated protein 3	*Dap3*	65111	6200176	2.01	1.85
Discs, large homolog 4 (*Drosophila*)	*Dlg4*	13385	1990669	3.42	3.42
Echinoderm microtubule-associated protein-like 4	*Eml4*	78798	780768	2.39	2.47
Ectonucleoside triphosphate diphosphohydrolase 2	*Entpd2*	12496	160411	1.91	2.04
Ectonucleotide pyrophosphatase/phosphodiesterase 5	*Enpp5*	83965	4850082	35.30	35.04
Elongation of very long chain fatty acids (FEN1/Elo2, SUR4/Elo3, yeast) -like 4	*Elovl4*	83603	1740424	2.42	2.75
Family with sequence similarity 171, member B	*Fam171b*	241520	7150026	2.73	2.95
FGFR1 oncogene partner 2	*Fgfr1op2*	67529	2490068	53.07	53.04
G-protein pathway suppressor 2	*Gps2*	56310	3400349	6.73	6.57
Hepatoma-derived growth factor	*Hdgf*	15191	1780608	3.75	3.27
Hermansky–Pudlak syndrome 6	*Hps6*	20170	5720291	3.54	3.52
Hypothetical protein LOC100043671	*LOC100043671*	100043671	3180379	2.50	2.18
Kinesin light chain 1	*Klc1*	16593	4050133	2.39	2.66
Kinesin light chain 1	*Klc1*	16593	6130468	10.46	10.99
Mannoside acetylglucosaminyltransferase 3	*Mgat3*	17309	3420504	4.22	4.75
Minichromosome maintenance deficient 6 (MIS5 homolog, *Schizosaccharomyces pombe*; *Saccharomyces cerevisiae*)	*Mcm6*	17219	270379	4.74	5.28
Minichromosome maintenance deficient 6 (MIS5 homolog, *S. pombe*; *Saccharomyces cerevisiae*)	*Mcm6*	17219	3290437	4.04	3.80
Mitochondrial ribosomal protein L48	*Mrpl48*	52443	1070482	7.28	4.85
Mitochondrial ribosomal protein L48	*Mrpl48*	52443	4920291	6.63	4.39
Mitochondrial ribosomal protein S27	*Mrps27*	218506	3800008	6.19	5.77
Mitochondrial translational release factor 1	*Mtrf1*	211253	4040286	3.09	3.02
Mpv17 transgene, kidney disease mutant-like	*Mpv17l*	93734	780215	28.51	29.32
Pentatricopeptide repeat domain 3	*Ptcd3*	69956	990326	8.23	9.00
Proline synthetase cotranscribed	*Prosc*	114863	5960414	9.85	9.27
Proteasome (prosome, macropain) subunit, β-type 6	*Psmb6*	19175	7650110	245.90	256.34
Protein phosphatase 1, regulatory (inhibitor) subunit 13B	*Ppp1r13b*	21981	430669	2.91	3.04
Rap guanine nucleotide exchange factor (GEF) -like 1	*Rapgefl1*	268480	1010524	5.17	5.52
Retinoblastoma binding protein 9	*Rbbp9*	26450	2230424	7.28	6.88
Ribosomal protein S15a	*Rps15a*	267019	6270092	9.71	8.56
Ribosomal protein S3	*Rps3*	27050	3400615	20.67	18.29
RIKEN cDNA 2700038C09 gene	*2700038C09Rik*	66496	4120068	1.59	1.60
RIKEN cDNA 3110035E14 gene	*3110035E14Rik*	76982	5340768	3.10	2.79
RIKEN cDNA 6330503K22 gene	*6330503K22Rik*	101565	3420521	8.77	7.10
Sema domain, 7 thrombospondin repeats (type 1 and type 1-like), transmembrane domain (TM) and short cytoplasmic domain, (semaphorin) 5A	*Sema5a*	20356	1660605	10.06	10.59
Sema domain, 7 thrombospondin repeats (type 1 and type 1-like), transmembrane domain (TM) and short cytoplasmic domain, (semaphorin) 5A	*Sema5a*	20356	6020274	11.36	11.00
Similar to Dullard homolog (*Xenopus laevis*)	*LOC100048221*	100048221	5360291	1.95	2.20
START domain containing 10	*Stard10*	56018	7570209	2.39	3.06
START domain containing 7	*Stard7*	99138	3180367	30.00	27.15
Sterol-C4-methyl oxidase-like	*Sc4mol*	66234	6420253	11.65	9.09
Higher					
Family with sequence similarity 20, member B	*Fam20b*	215015	7570671	4.31	3.92
γ-Aminobutyric acid (GABA-A) receptor, subunit-β3	*Gabrb3*	14402	4010452	2.07	2.60
Gene model 962	*Gm962*	381201	5360193	3.56	3.42
High-mobility group nucleosomal binding domain 2	*Hmgn2*	15331	610600	1.97	2.71
Similar to Ubc protein	*LOC100048105*	100048105	2260521	1.85	1.82
Transmembrane protein 66	*Tmem66*	67887	4120220	8.15	7.78
Transmembrane protein 87A	*Tmem87a*	211499	3390341	7.46	2.12

Forty-seven probes had significantly lower signal (false discovery rate = 0.001, fold change ≥ 1.5) in DBA than SJL and B6, and seven probes had significantly higher signal (false discovery rate = 0.001, fold change ≥ 1.5) in DBA than SJL and B6.

Table S2. Characteristics of autopsy-confirmed brain samples

	Definitive AD (n = 10)	Control subjects (n = 14)	P value
Age mean ± SD	87.4 ± 6.95	88.7 ± 5.73	0.62
Sex (male/female)	3/7	3/11	0.67

P values were assessed by t and Fisher exact tests. AD, Alzheimer's disease.

Table S3. Characteristics of peripheral lymphocyte samples

	Patients with AD (n = 47)	Control subjects (n = 17)	P value
Age mean ± SD	69.0 ± 10.3	58.2 ± 15.5	0.0047
Sex (male/female)	12/35	6/11	0.53
APOE-ε4 carrier/noncarrier	26/21	5/12	0.091

P values were assessed by t and Fisher exact tests. AD, Alzheimer's disease.